Synchronous coherent population trapping and its magnetic spectral response in rubidium vapor

Gour S. Pati, Renu Tripathi, Raghwinder S. Grewal, Mauricio Pulido, and Robin A. Depto

Phys. Rev. A **104**, 033116 — Published 24 September 2021

DOI: 10.1103/PhysRevA.104.033116

Synchronous coherent population trapping and its magnetic spectral response in rubidium vapor

Gour S. Pati*, Renu Tripathi, Raghwinder S. Grewal, Mauricio Pulido, and Robin A. Depto

Division of Physics, Engineering, Mathematics and Computer Science
Delaware State University, Dover, DE 19901, USA

This paper reports experimental investigations of the spectral response of synchronous coherent population trapping (CPT) for magnetometry applications. Synchronous CPT is demonstrated using resonant two-photon excitation with a modulated bichromatic laser field in the ^{87}Rb D_1 manifold. Spectra containing multiple magnetic resonances are produced due to two-photon excitations created by various frequency components of the modulated beam. Theoretical modeling based on the atomic density-matrix equations is used to simulate the spectral response of synchronous CPT. Our results show potential advantages of synchronous CPT over synchronous optical pumping (SOP) for magnetic field measurement. Magnetic resonances signals produced by synchronous CPT can be used in eliminating dead-zone problem and also, used in determining the magnetic field direction.

I. INTRODUCTION

Optical magnetometers measure magnetic field by utilizing ground-state coherence in alkali atoms produced by resonant excitation with a polarized optical field [1-3]. For instance, resonant excitation of atoms with linearly polarized light in a zero magnetic field can create a dark state superposition between ground-state sublevels satisfying the coherence condition $|\Delta m_F| = 2$, where $|\Delta m_F|$ corresponds to the change in magnetic quantum number between the ground-state sublevels. This is known as the Hanle effect or alternatively, as coherent population trapping (CPT) resulting from the intra-hyperfine ground-state sublevels. The line shapes of Hanle resonance have been studied analytically using density-matrix equations [3]. The Hanle effect has been widely studied in magnetometry for measuring weak magnetic fields (i.e. $B \approx 0$) with high sensitivities [4-6]. On the other hand, optical magnetometers can measure strong magnetic fields (e.g. fields ranging from micro-gauss level to beyond the strength of earth's magnetic field) by using synchronous optical pumping (SOP) of atoms [7-13]. In this case, light is modulated at the Larmor frequency, Ω_L to create a resonant buildup in the ground-state coherence. Multiple magnetic resonances can be produced in the SOP spectrum depending on the choice of light polarization, interaction geometry (i.e. the angle between the light propagation direction and the B field), and also modulation duty cycle of light [13,14]. Grujić and Weis studied the features of magnetic resonance spectra produced using SOP with modulated circularly polarized light in a transverse magnetic field [15]. Breschi *et al* have demonstrated push-pull optical pumping in conjunction with SOP based atomic magnetometry [16]. Generally speaking, contrast in SOP resonances can be reduced due to loss of atomic population through spontaneous emission to the other ground-state in the open ^{87}Rb D_1 transitions. However, a weak resonance corresponding to a higher-order coherence condition $|\Delta m_F| = 4$ has also been observed in SOP by using higher light power and nonlinear magneto-optical rotation measurement [13].

In this paper, we discuss a method, termed as synchronous CPT, which, in contrast to SOP, produces strong magnetic resonances by simultaneous two-photon excitation from both hyperfine ground-states [i.e. $|F = 1\rangle$ and $|F = 2\rangle$] in ^{87}Rb D_1 line using a modulated bichromatic laser field. The proposed method can give reduced light shift compared to SOP and therefore, higher accuracy in the magnetic field measurement. Implementation of synchronous CPT is different from the commonly used CPT scheme which is utilized in atomic clock [17,18] and magnetometry [19,20], where a continuous laser produces the CPT resonance. In a recent study, we showed the advantage of synchronous CPT for remote magnetometry using sodium D_1 line fluorescence measurement [21]. Magnetic resonances in synchronous CPT are produced due to coherence created between the inter-hyperfine ground-state sublevels by the spectral components of the

*gspati@desu.edu

modulated beam. Here, we show that synchronous CPT can produce multiple high-contrast magnetic resonances in ^{87}Rb D_1 line, and the spectral features of these resonances are different from those produced by conventional CPT. Resonances in synchronous CPT are produced at positions which are dependent on the laser modulation frequency and the magnetic field. Unlike conventional CPT based magnetometry which requires a measurement of microwave frequency [19,20], the field strength B in synchronous CPT can be directly measured from the resonant modulation frequency.

We have investigated, both experimentally and theoretically, the spectral response of synchronous CPT in ^{87}Rb D_1 manifold using resonant two-photon excitation with $|F' = 2\rangle$ and $|F' = 1\rangle$ excited states. Theoretical investigations are performed using atomic density-matrix calculations simulating the interaction of multi-level ^{87}Rb atoms with the modulated bichromatic laser field. Experiments are performed in a pure-isotope ^{87}Rb vapor cell kept in a high magnetic-shield environment. Spectral characteristics of synchronous CPT are compared with its counterpart SOP. Our study shows that synchronous CPT produces a strong magnetic resonance peak at $2\Omega_L$ using circular light polarization and longitudinal B field applied parallel to the light propagation direction, whereas SOP cannot produce any resonant response under this condition. Multiple resonances are also produced by synchronous CPT when the applied B field is inclined towards the plane of light polarization. We explain the origin of these resonances using multiple Λ −systems formed in the ^{87}Rb D_1 manifold. Our findings suggest that synchronous CPT method can be further developed in realizing dead-zone-free magnetometry, as well as vector magnetometry. The remainder of this paper is organized as follows. In Sec. II, the experimental setup is described. In Sec. III, we discuss the theoretical model and the origin of magnetic resonances produced by synchronous CPT using Λ −systems. Finally, in Sec. IV, we provide the results and discussion, drawing comparisons between synchronous CPT and SOP, and emphasizing the advantages of synchronous CPT in magnetometry.

II. EXPERIMENT

Figure 1 shows the layout of our experimental apparatus for synchronous CPT. We used a diode laser (linewidth < 1 MHz) tuned to resonance with the rubidium D_1 line ($\lambda \simeq 795$ nm). The laser beam is modulated by a high-frequency (GHz) electro-optic modulator (EOM) which is driven by a microwave generator for producing first-order optical sidebands with frequency shifts $\Delta_s = \pm \nu_{hfs}/2$, where $\nu_{hfs} \simeq 6.8347$ GHz is the ground-state hyperfine frequency of ^{87}Rb. The two first-order EOM sidebands create a bichromatic laser field for our synchronous CPT experiment causing two-photon excitation in ^{87}Rb hyperfine $|F = 1\rangle$ and $|F = 2\rangle$ ground-states. The EOM bias voltage is actively controlled for minimizing the carrier [18]. The amplitudes of higher-order EOM sidebands are also suppressed by nearly 10 dB (with respect to the first-order sidebands) by controlling the drive voltage from the microwave generator. A fraction of the laser beam after the EOM is sent through a reference rubidium cell for laser frequency stabilization. The laser is locked to a frequency corresponding to the minimum transmission (or maximum absorption) point created by the two first-order EOM sidebands in the Doppler absorption spectrum [18]. This way, the first-order EOM sidebands get simultaneously resonant with the transitions from $|F = 1\rangle$ and $|F = 2\rangle$ ground-states to a common excited state (i.e. either $|F' = 1\rangle$ or $|F' = 2\rangle$) in the ^{87}Rb D_1 line. The laser beam after the EOM is amplitude-modulated using a low-frequency (MHz) acousto-optic modulator (AOM1), thus, creating a modulated bichromatic laser excitation for the synchronous CPT experiment. The AOM1 is driven by periodic 80 MHz RF pulses generated from an RF generator, supplied with a square-wave modulation input of frequency Ω_m from an arbitrary waveform generator (AWG). As the amplitude-modulated diffracted light produced by AOM1 is frequency-shifted by 80 MHz from the original laser frequency, this frequency shift is compensated in the laser stabilization setup by using an identical 80 MHz AOM2 driven by an unmodulated 80 MHz RF signal, as shown in Fig. 1. This keeps the laser stabilization in a continuous mode for maintaining the laser lock.

A pure isotope ^{87}Rb vapor cell (path length $= 5$ cm and diameter $= 2.54$ cm) containing Ne buffer gas at 10 Torr pressure is used in our experiments. The cell is heated to a steady temperature of 45^oC, which gives an atomic density $\simeq 10^{11}$ atoms/cm^3. To create non-magnetic cell heating, AC current at 50 kHz is sent through the heating coils which are made from twisted nichrome wires. The Rb cell is placed inside a

magnetic shield enclosure (with approximately 50 dB shielding factor) consisting of four nested mu-metal layers. A three-axis cylindrical field coil is used inside the innermost layer of this mu-metal enclosure for cancelling any residual magnetic field inside and for applying a controlled magnetic field in any arbitrary direction. The field coil inside the magnetic shield enclosure produces a uniform magnetic field over 1 cm length along the x/y directions and about 3 cm along z-direction. Since our vapor cell dimension is bigger, small magnetic field gradients are present along all three dimensions of the vapor cell. The field coil is connected to three independent low-noise voltage-controlled current sources, to have the flexibility of applying independent magnetic fields, namely, B_x, B_y and B_z along the x, y and z directions respectively.

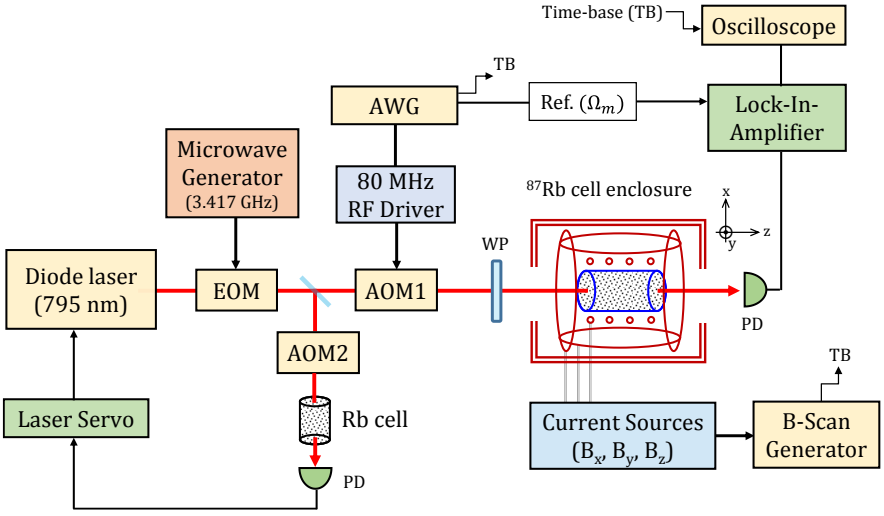

FIG. 1. Experimental setup for synchronous CPT. Laser frequency is stabilized using the absorption signal produced by the bichromatic laser beam passing through a reference rubidium (Rb) cell. WP: waveplate (HWP/QWP), PD: photodiode and TB: time base.

The (x,y,z) coordinate system chosen to describe our experiment is shown (close to cell enclosure) in Fig. 1. Longitudinal magnetic field B_z in our experiments is continuously varied (or scanned) by using a voltage scan generator connected to the current source in the z-direction. The laser beam after AOM1 is expanded to approximately 8 mm in diameter, and polarized (either circularly or linearly) by using a quarter-waveplate (QWP) or a half-waveplate (HWP), as needed. Expanded beam size and frequent collisions of ^{87}Rb atoms with buffer Ne atoms in the vapor cell help in preventing transit-time broadening of the magnetic resonances produced by the synchronous CPT process. We measure the spectral response of synchronous CPT by demodulating the photodiode voltage output at modulation frequency Ω_m using a lock-in-amplifier (LIA). Both in-phase (I) and quadrature (Q) components of the spectral response are acquired from two LIA channels.

III. ATOMIC MODEL

We developed a theoretical model using the atomic density-matrix equations [22] to study the magnetic spectral response of synchronous CPT in ^{87}Rb D_1 line under different excitation conditions. The results obtained from our theoretical model are compared with our experimental results obtained under the same excitation conditions. The modulated bichromatic laser field in the model is defined as

$$\vec{E}(t) = \vec{E}_1 + \vec{E}_2 = \sum_{i=1}^{2} \hat{e}_L E_{0i}[1 + M\,\xi(t)]e^{-i\omega_i t} + c.c. \qquad (1)$$

where $\hat{e}_L$ represents the polarization of two co-polarized laser fields $\vec{E}_1$ and $\vec{E}_2$ (i.e. the first-order EOM sidebands) with respective amplitudes E_{01} and E_{02} and frequencies ω_1 and ω_2, M corresponds to the

modulation depth, and $\xi(t)$ represents a periodic square-wave modulation function of frequency Ω_m. The square-wave light modulation $\xi(t)$ is described in our model by using the Fourier series expansion as

$$\xi(t) = \sum_m g_m(\eta)\, cos(m\,\Omega_m t), \qquad m = 1,2,... \tag{2}$$

where Fourier coefficients $g_m(\eta) = \frac{2}{m\pi} sin(m\pi\eta)$ and η is the duty cycle of $\xi(t)$. Integer index m corresponds to different harmonic functions $cos(m\,\Omega_m t)$ in the Fourier series, and g_m represents the amplitude of m[th] harmonic. The spectral components of the modulated bichromatic laser field in Eq. (1) consist of two prime frequencies ω_1 and ω_2 and multiple frequency harmonics with frequencies corresponding to $\omega_i \pm m\Omega_m,\ i = 1,2$. Synchronous CPT is realized by matching the frequency difference $(\omega_1 - \omega_2)$ with $\omega_{hfs}[= 2\pi(\nu_{hfs})]$. This condition can also be termed as zero difference detuning (or two-photon detuning) $\Delta\ [= (\omega_1 - \omega_2) - \omega_{hfs}] = 0$. For our discussions, we will utilize two energy diagrams (as shown in Fig. 2) depicting possible $\Lambda-$systems formed by various frequency components of a

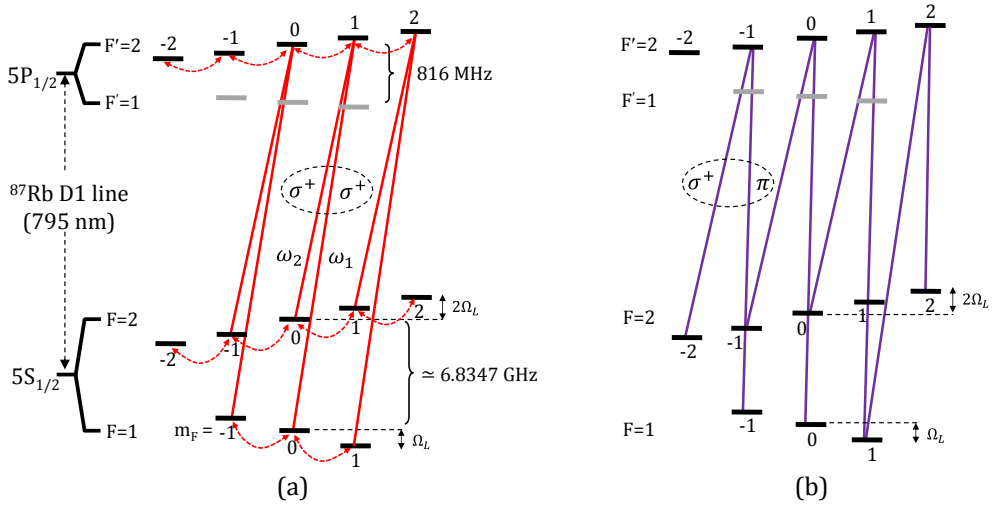

Fig. 2. Energy diagrams showing $\Lambda-$systems formed due to interaction of the modulated bichromatic σ^+ polarized laser field with ^{87}Rb D_1 manifold in the presence of a magnetic field $\vec{B}$. Resonant two-photon excitation with $|F' = 2\rangle$ excited state is considered here. The formation of $\Lambda-$systems in Fig. 2a are shown by considering the z-axis as the quantization axis, and in Fig. 2b, by considering direction of $\vec{B}$ as the quantization axis. In Fig. 2(b), $\Lambda-$systems formed by the (σ^+, π) combination are shown. Resonant frequency for each $\Lambda-$system can be inferred from the diagrams.

modulated bichromatic σ^+ polarized laser field in the ^{87}Rb D_1 manifold, in the presence of a magnetic field $\vec{B}$. The $\Lambda-$systems are formed when $\Delta = 0$ and the laser modulation frequency Ω_m coincides with $\pm\Omega_L, \pm 2\Omega_L$ and $\pm 3\Omega_L$, where Ω_L corresponds to the Larmor frequency (or ground-state Zeeman splitting) in ^{87}Rb, as shown. These $\Lambda-$systems are responsible for producing multiple magnetic resonances, due to coherence created by dark superposition between the hyperfine ground-state sublevels. The $\Lambda-$system corresponding to $(0,0)$ ground-state superposition is formed by resonant two-photon excitation ($\Delta = 0$) with frequencies ω_1 and ω_2. In Fig. 2(a), we have considered the z-axis (or light propagation direction) as the quantization axis, as used in our model. Thus, the $\Lambda-$systems are formed by σ^+ transitions corresponding to $\Delta m_{FF'} = +1$. Three possible $\Lambda-$ systems corresponding to $(-1,-1)$, $(0,0)$ and $(+1,+1)$ superposition states are shown in this figure. The interaction of the magnetic field $\vec{B}$ in this case is modeled using an interaction Hamiltonian $\hat{H}_{IB} = g_F \mu_B \vec{F} \cdot \vec{B}$, where g_F is the Landé g-factor, $\mu_B \simeq \hbar(1.4\ \mathrm{MHz/G})$ is the Bohr magneton, $\hbar$ is the reduced Planck's constant, and $\vec{F}$ corresponds to the total angular momentum

of the state. For an arbitrary $\vec{B} = B_x\,\hat{x} + B_y\,\hat{y} + B_z\,\hat{z}$, the element of $\hat{H}_{IB}$ in the ground-state $|F, m_F\rangle$ is given by

$$\begin{aligned}\langle F, m_F|\hat{H}_{IB}|F, m_F'\rangle \\ &= \alpha_F \left\{\frac{B_x}{2}\left[\{F(F+1) - m_F'(m_F'+1)\}^{\frac{1}{2}}\,\delta_{\{m_F,(m_F'+1)\}}\right.\right. \\ &\left. + \{F(F+1) - m_F'(m_F'-1)\}^{\frac{1}{2}}\,\delta_{\{m_F,(m_F'-1)\}}\right] \\ &- \frac{iB_y}{2}\left[\{F(F+1) - m_F'(m_F'+1)\}^{\frac{1}{2}}\;\delta_{\{m_F,(m_F'+1)\}}\right. \\ &\left.\left. - \{F(F+1) - m_F'(m_F'-1)\}^{\frac{1}{2}}\,\delta_{\{m_F,(m_F'-1)\}}\right] + B_z m_F'\delta_{\{m_F,m_F'\}}\right\}\end{aligned} \tag{3}$$

Here, $\alpha_F = g_F\mu_B$ and δ is the Kronecker delta function. The elements of $\hat{H}_{IB}$ for the excited state sublevels $|F', m_{F'}\rangle$ can be calculated by replacing corresponding F, m_F and α_F by F′, $m_{F'}$ and $\alpha_{F'}(= g_{F'}\mu_B)$ in the above equation. Equation (3) indicates that the magnetic field component B_z, parallel to the quantization axis, produces a Zeeman shift, and magnetic field components B_x and B_y, perpendicular to the quantization axis, produce couplings between neighboring Zeeman sublevels as shown by 'dashed arrows' in Fig. 2(a). Coupling coefficients for B_x and B_y can be calculated from Eq. (3). A Hamiltonian describing the interaction of the magnetic field $\vec{B}$ with the ^{87}Rb atoms, is constructed in our model using this equation. Intuitively, one can imagine new Λ −systems being formed due to couplings introduced by B_x and B_y. Nevertheless, it is difficult to visualize all possible Λ −systems in Fig. 2(a). Instead, we show formation of additional Λ −systems in Fig. 2(b) by considering the direction of $\vec{B}$ as the quantization axis. In this interaction picture, a σ^+ polarized laser field can be transformed into the $\vec{B}$ basis and can be shown to contain π and σ^- polarization components as well. Figure 2(b) shows Λ −systems that could be formed due to a combination of (σ^+, π) transition. We do not show the Λ −systems formed by a combination of (σ^-, π) transitions since they could be imagined to be antisymmetric (i.e. with a negative resonant frequency) with respect to that for (σ^+, π) combination. In essence, multiple magnetic resonances are formed in synchronous CPT by these Λ −systems. The strength of a particular resonance is decided by the strengths of corresponding σ^+, σ^- and/or π transitions associated with it.

There are two important differences between magnetic resonances produced by synchronous CPT and SOP. First, the $\pm 3\,\Omega_L$ resonances generated in synchronous CPT, could not be generated in SOP as the later uses a single-frequency laser excitation forming Λ −systems within only one of the hyperfine ground-states [15]. Second, unlike SOP, synchronous CPT can always produce a resonant response irrespective of the laser polarization and the magnetic field orientation due to the involvement of two hyperfine ground-states with opposite signs for respective gyromagnetic ratios. We accurately model the spectral response of synchronous CPT using the following atomic density-matrix equation [22]:

$$\frac{\partial \rho}{\partial t} = -\frac{i}{\hbar}\left[\hat{H}, \rho\right] + \hat{L}\rho \tag{4}$$

Here ρ represents the density operator, $\hat{H}$ represents the total Hamiltonian of the atomic system, and $\hat{L}$ represents the combined source (or population transfer) and transverse-decay (or dephasing) matrices. The diagonal terms in the $\hat{L}$ matrix correspond to population transfer, and the off-diagonal terms in the $\hat{L}$ matrix correspond to dephasing accompanied by population decay and other phenomenological relaxation processes. All radiative decay channels from the excited-state sublevels to the ground-state sublevels using σ^+, σ^-, and π transitions are considered in this $\hat{L}$ matrix. The Hamiltonian, $\hat{H} = \hat{H}_A + \hat{H}_{IE} + \hat{H}_{IB}$, is expressed as the sum of three parts using the electric dipole approximation, rotating wave approximation, and rotating wave transformation. $\hat{H}_A$ represents the internal atomic energy, $\hat{H}_{IE}\left(= \vec{d}\cdot\vec{E}\right)$ represents the interaction with the bichromatic modulated laser field described in Eq. (1), and $\hat{H}_{IB}$ represents the

interaction with the magnetic field $\vec{B}$ described by Eq. (3). Elements of $\hat{H}_{IE}$ are defined in terms of Rabi frequencies $\Omega_i = \langle F, m_F \| d_i \| F', m_{F'} \rangle E_i/\hbar$, $i = 1,2$ of the laser fields at frequencies ω_1 and ω_2 for the $|F, m_F\rangle \rightarrow |F', m_{F'}\rangle$ transition, and d_i corresponds to the dipole operator. Light modulation is incorporated in the model by modulating the Rabi frequencies Ω_i using the harmonic modulation function described in Eq. (2), by keeping terms up to the eighth harmonic. Time-dependent density-matrix equations in Eq. (4) are solved numerically [18,22,23] to calculate the spectral response using a normalized transmissivity function defined by the relation $T \simeq \left(1 - \sum_{|e_i\rangle|g_j\rangle} Im\left[\langle e_i|\rho|g_j\rangle\right]\right)$, where $|e_i\rangle$ and $|g_j\rangle$ are the excited-state and the ground-state sublevels involved in the optical transition. The in-phase and quadrature components of the resonance spectrum are calculated by demodulating T at the light modulation frequency Ω_m. Our model includes following simplifications to reduce the computation time. Interaction with only one excited state (i.e. either $|\mathrm{F}' = 1\rangle$ or $|\mathrm{F}' = 2\rangle$) is considered in our model. This does not have a significant impact on our results since the excluded excited state in the ^{87}Rb D_1 line is highly detuned by nearly $816\ MHz$ which is greater than the Doppler width $\simeq 500\ MHz$. Effects of velocity averaging due to atomic motion and spatial laser intensity distribution are not considered in our model. We calculated the spectral response of synchronous CPT using this model for validating our experimental results.

IV. RESULTS AND DISCUSSION

In this section, we compare the spectral responses produced by synchronous CPT with its counterpart SOP. The spectral acquisition is performed in two different ways: a) by varying the B field while keeping the laser modulation rate fixed, and b) by varying the laser modulation rate while keeping the B field fixed. Before presenting these results, we show the conventional CPT spectra produced in the presence of B field.

A. CPT spectra in the presence of a B field

The spectral response of conventional CPT is acquired by using a continuous bichromatic laser beam with σ^+ polarization. In this case, the laser modulation is kept off (i.e. by switching AOM1 off in the experiment [Fig. 1]) to produce a continuous beam. The laser is stabilized and frequencies ω_1 and ω_2 create resonant two-photon excitation in the hyperfine ground states via $|\mathrm{F}' = 2\rangle$ excited state in ^{87}Rb D_1 line. CPT spectra are obtained by changing difference detuning Δ around zero value, which is achieved by changing the EOM drive frequency around $\nu_{hfs}/2 \simeq 3.4173$ GHz. Figure 3(a) shows CPT spectra in the presence of different B fields. The spectra shown in Fig. 3(a) contain a central CPT resonance with peak at $\Delta = 0$ and multiple Zeeman CPT resonances with peaks at $\Delta = \pm\Omega_L, \pm 2\,\Omega_L$ and $\pm 3\,\Omega_L$, where $\Omega_L = \gamma B$ with the total magnetic field $B = \sqrt{B_x^2 + B_y^2 + B_z^2}$ and γ is the atom gyromagnetic ratio ($\simeq 7$ Hz/nT for ^{87}Rb). Magnetic field can be measured from the peak Δ value corresponding to any one of the Zeeman CPT resonances [17,24]. However, a measurement of B from the peak Δ value requires an estimation of ν_{hfs} which could get dynamically perturbed by multiple sources including the buffer gas induced shift. Figure 3(a) shows that a longitudinal magnetic field B_z creates $\pm 2\,\Omega_L$ CPT resonances, whereas the transverse field B_x (and/or B_y) produces $\pm\Omega_L, \pm 3\,\Omega_L$ CPT resonances. The origins of these resonances were explained in Section III using $\Lambda-$systems. Peak amplitudes of CPT resonances for positive Δ values are found to be higher than those for negative Δ values. This is due to optical pumping caused by σ^+ polarization, which gives rise to higher population in positive m_F Zeeman sublevels. A symmetric CPT spectral response (not shown here) is produced when a bichromatic laser field with linear polarization (i.e. $lin \parallel lin$) is used [18,24]. Figure 3(b) shows the corresponding theoretical CPT spectra (with similar asymmetry in peak amplitude distribution) obtained by solving the density-matrix equations in Eq. (4) under a steady-state condition, i.e. $\frac{\partial \rho}{\partial t} = 0$. Discrepancies observed in peak amplitudes and spectral backgrounds between experiment [Fig. 3(a)] and theory [Fig. 3(b)] are due to simplifications used in our model. We measured the linewidths of CPT resonances using a Lorentzian fitting function. The central CPT resonance

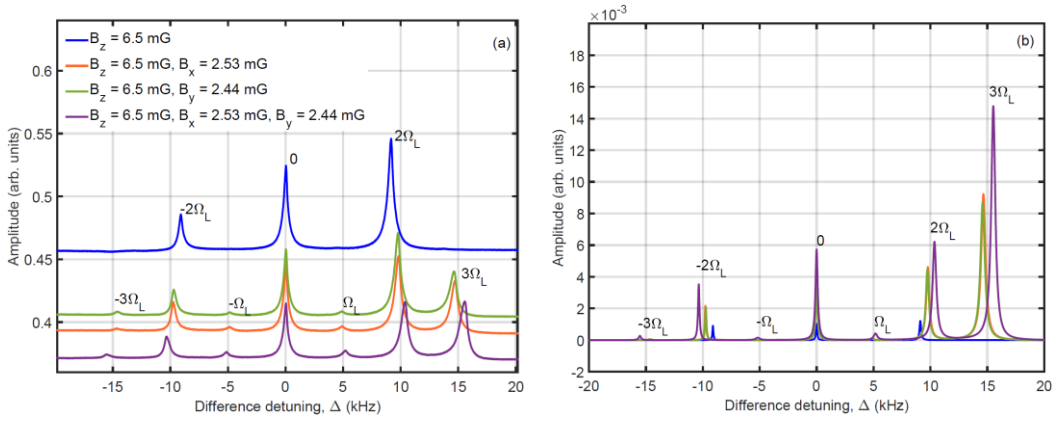

Fig. 3. (a) Experimental CPT spectra acquired using continuous resonant two-photon excitation with $|F' = 2\rangle$ excited state and σ^+ polarized light fields. Fig. 3(b) Theoretical CPT spectra calculated using similar excitation conditions as in the experiment. A total optical power of 100 μW is used in the laser beam. Different colors in CPT spectra are chosen for different external magnetic fields. The following parameters are used in our simulations: $\Omega_1 = \Omega_2 = \Gamma/180$ and spontaneous decay rate $\Gamma = 6$ MHz for ^{87}Rb atoms.

is insensitive to magnetic field and has a linewidth of approximately 209 Hz. Due to the presence of a small magnetic field inhomogeneity in our experiment, the magnetically sensitive $\Omega_L, 2\Omega_L$ and $3\Omega_L$ CPT resonances have broader linewidths of approximately 305 Hz, 318 Hz and 371 Hz, respectively. In our theoretical model, we assumed equal Rabi frequencies for laser frequencies ω_1 and ω_2 (i.e. $\Omega_1 = \Omega_2 = \Gamma/180$), where Γ corresponds to the spontaneous decay rate of the atom. The linewidths of CPT resonances in Fig. 3(b) were also estimated and found to match approximately with the expected power-broadened CPT linewidth $\Omega^2/\Gamma \simeq 185$ Hz, where $\Omega = \sqrt{(|\Omega_1|^2 + |\Omega_2|^2)/2}$ is the average Rabi frequency [18]. Interestingly, linewidths of $\Omega_L, 2\Omega_L$ and $3\Omega_L$ CPT resonances obtained from theory [Fig. 3(b)] differed from 185 Hz slightly, since the actual linewidth of CPT resonance depends on the dipole matrix elements associated with the two legs of Λ −system.

B. Synchronous CPT spectra in the B field domain

Here, we show the spectral response of synchronous CPT produced by using a modulated bichromatic laser beam with a fixed modulation frequency $\Omega_m = 10$ kHz, 50% duty cycle (i.e., $\eta = 0.5$ corresponds to square-wave modulation with missing even-order sidebands) and σ^+ polarization. The laser frequencies ω_1 and ω_2 (i.e., the first-order EOM sidebands) are adjusted to keep the detuning $\Delta = 0$ while being on resonance with the $|F' = 2\rangle$ excited state. Figures 4(a,b) show the magnetic resonance spectra obtained by varying the longitudinal magnetic field B_z (or $\Omega_L = \gamma B_z$) around zero. Both in-phase (I) and quadrature (Q) components of the spectra [Figs. 4(a,b)] are measured using the lock-in-amplifier. These I and Q components yield information about amplitude and phase of the resonance signal, respectively. The I component shows multiple resonance peaks, and the Q component shows phase dispersions associated with the resonances caused by synchronous CPT. Figures 4(c,d) show respective I and Q components of the theoretical resonance spectra obtained by numerically solving the time-dependent density-matrix equations described in Eq. (4). These results show good agreement with Figs. 4(a,b). Magnetic resonances with peaks corresponding to $\Omega_L = \pm\Omega_m/2$ are produced by the longitudinal field B_z. The quadrature components of $\pm\Omega_m/2$ resonances have opposite signs for phase dispersion. Resonances at zero field (i.e. $\Omega_L = 0$) are formed by multiple superpositions of degenerate ground state sublevels and therefore, do not show any phase dispersion in the Q component [Figs. 4(b,d)]. For comparison, we also present an analogous SOP spectra in Fig. 4 obtained by using a fixed non-zero value of Δ (= 68 kHz), thus creating single-photon excitation conditions separately from two ground-states with two laser frequencies ω_1 and ω_2. A SOP uses

a single laser field instead of two laser fields as is the case here. The second field in this situation, acts as a repump. Thus, the SOP condition in our case, more specifically resembles SOP with repump [25]. For $\Delta = 68$ kHz case, the two first-order sidebands produced by the EOM serve as pump and repump for SOP.

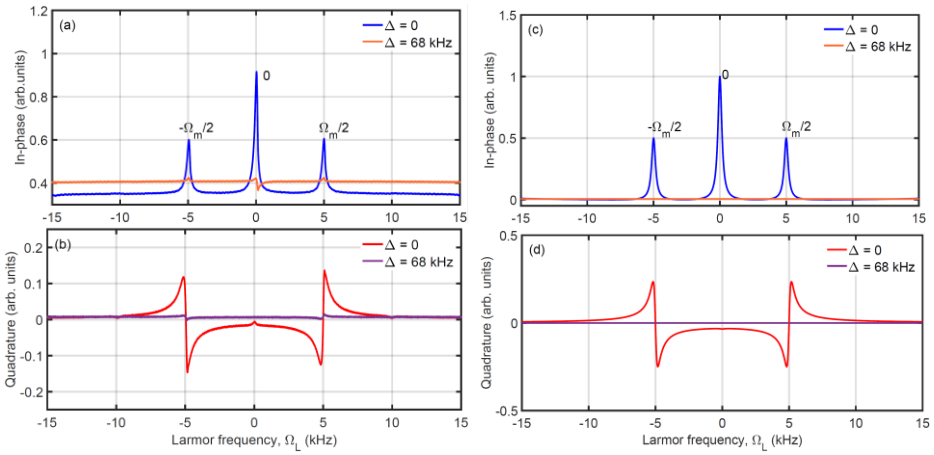

Fig. 4. (a,b) Experimental magnetic resonance spectra (I and Q components) acquired by scanning the longitudinal field B_z (or Ω_L) around zero value. A modulated bichromatic laser beam ($\Omega_m = 10$ kHz and 50% duty cycle) with σ^+ polarization and in resonance with $|F' = 2\rangle$ excited state is used. Fig. 4(c,d) Magnetic resonance spectra calculated using our theoretical model. Difference detuning $\Delta = 0$ corresponds to synchronous CPT and $\Delta = 68$ kHz is considered analogous to SOP. Parameters used in our simulations are the same as those in Fig. 3.

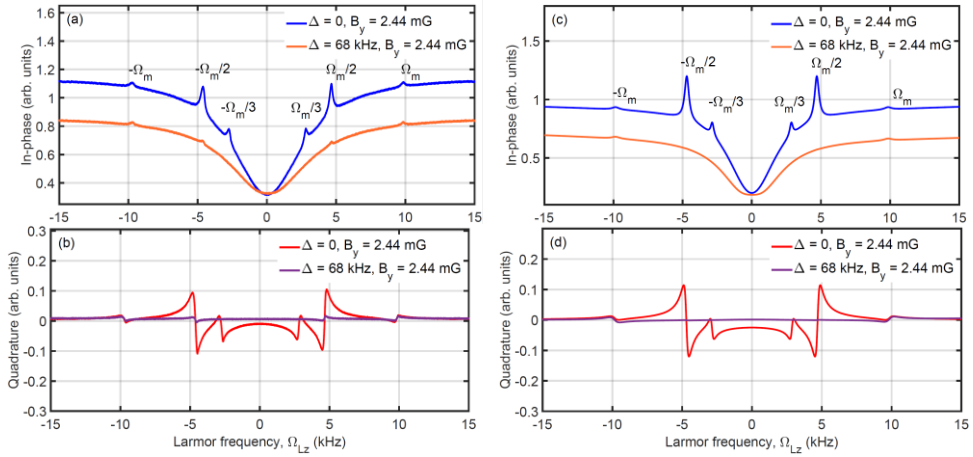

Fig. 5. (a,b) Experimental magnetic resonance spectra acquired by scanning the longitudinal field B_z and simultaneously applying a constant transverse field $B_y (= 2.44$ mG). Fig. 5(c,d) Corresponding spectra calculated using our theoretical model. A modulated bichromatic laser beam ($\Omega_m = 10$ kHz and 50% duty cycle) with σ^+ polarization and in resonance with $|F' = 2\rangle$ excited state is used.

The spectra in Figs. 4 do not show any resonance for longitudinal field B_z. This confirms the vector nature of SOP resonance for which longitudinal field is a dead-zone [14]. This can be eliminated by employing a polarization modulation scheme which can simultaneously create SOP resonances in both alignment and orientation [26]. However, the implementation of a suitable polarization modulation scheme could be quite complicated. Instead, our result shows that this dead-zone problem can be (quite conveniently) avoided in synchronous CPT by using the strong CPT resonant responses at $\Omega_L = \pm\Omega_m/2$ produced by σ^+ polarization.

Figure 5 (a,b) shows the experimental magnetic resonance spectra produced by synchronous CPT when a constant transverse field $B_y(= 2.44\ \text{mG})$ is applied along with a varying longitudinal field B_z. For comparison, we kept all other experimental and simulation parameters same as the ones reported in Fig. (4). The I and Q components of the resonance spectra are shown as a function of $\Omega_{\text{Lz}}(= \gamma B_z)$. Unlike those in Fig. 4, the location of a particular resonance peak in Fig. 5 is determined by matching $\Omega_{\text{m}}(= 10\ \text{kHz})$ or its subharmonic with the total Larmor frequency $\Omega_{\text{L}}(= \gamma B = \gamma\sqrt{\text{B}_y^2 + \text{B}_z^2})$. In addition to magnetic resonances at $\Omega_{\text{L}} = \pm\Omega_m/2$, resonances at $\Omega_{\text{L}} = \pm\Omega_m/3$ and $\pm\Omega_m$ are also produced in this case due to the presence of weak π and σ^- transitions which are created by the transverse field B_y. Resonances at $\pm\Omega_m/3$ are produced due to dark superposition of inter-hyperfine Zeeman end-states, as described earlier in section III. Figures 5(c,d) show the spectra calculated using our theoretical model, which are in good

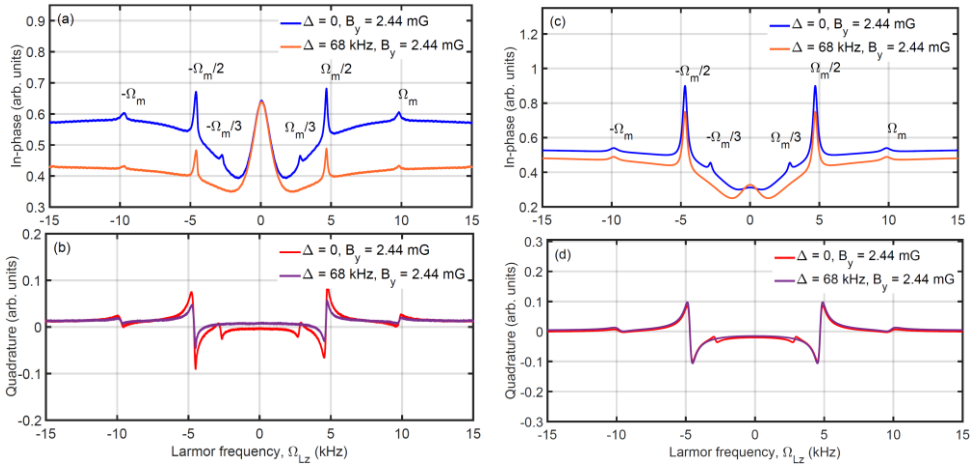

Fig. 6. (a,b) Experimental magnetic resonance spectra obtained by using a modulated laser beam ($\Omega_{\text{m}} = 10$ kHz and 50% duty cycle) with 45^0 linear polarization and in resonance with $|\text{F}' = 1\rangle$ excited state in ^{87}Rb D_1 manifold. (c,d) Spectra calculated using our theoretical model. A constant transverse field $B_y(= 2.44\ \text{mG})$ is applied and the longitudinal field B_z is scanned over the same range as in Fig. 5.

agreement with the experiment [Figs. 5(a,b)]. The quadrature components in Figs. 5(b,d) show phase dispersions associated with all resonances. Figures 5(a,b) also include equivalent SOP (i.e. SOP with repump) spectral responses for $\Delta = 68$ kHz. In this case, only one pair of very weak SOP resonances at $\Omega_{\text{L}} = \pm\Omega_m$ are produced in the spectrum. This matches with our theoretical results shown in Figs. 5(c,d). Due to imperfectness in the σ^+ polarization, weak SOP resonances at $\Omega_{\text{L}} = \pm\Omega_m/2$ are also produced in the experiment [Fig. 5(a)]. Please note that unlike Fig. 4, a sharply peaked zero-field magnetic resonance could not be observed at the center. This is because a true zero-field condition does not exist in this case due to the presence of transverse field B_y. On the other hand, the presence of B_y introduces a coupling between the neighboring ground-state sublevels (discussed in Section III) which leads to a spectrally broadened absorption dip at the center [Figs. 5(a,c)].

We have also studied the spectral response of synchronous CPT using resonant excitation with $|\text{F}' = 1\rangle$ excited state in ^{87}Rb D_1 line. In this case, a modulated bichromatic laser beam ($\Omega_{\text{m}} = 10\ kHz$ and 50% duty cycle) with 45^0 linear polarization is used. Linear polarization is found to produce stronger resonances compared to σ^+ polarization used previously for excitation of $|\text{F}' = 2\rangle$ state. Fig. 6 shows the magnetic resonance spectra obtained by applying a constant transverse field $B_y\ (= 2.44\ \text{mG})$ and a varying longitudinal field B_z over the same range as used in Fig. 5. The experimental spectra [Figs. 6 (a,b)] for synchronous CPT (i.e., $\Delta = 0$) contain magnetic resonances with peaks at $\Omega_{\text{L}} = \pm\Omega_m/3\ , \pm\Omega_m/2$ and

$\pm\Omega_m$, which are produced by σ^+, $\sigma^-$and π components associated with the linearly polarized laser fields. Figures 6(c,d) show our theoretical results which are in good agreement with the experiment. Peak amplitudes of $\Omega_L = \pm\Omega_m/2$ resonances (generated primarily due to B_z) are found to be larger compared to $\Omega_L = \pm\Omega_m/3$ and $\pm\Omega_m$ resonances. This is due to strong σ^+ and σ^- components of the linearly polarized laser field. The spectral response for analogous SOP with repump ($\Delta = 68$ kHz) shows resonances at $\Omega_L = \pm\Omega_m$ and $\Omega_L = \pm\Omega_m/2$. Population transfer by the repump beam increases the contrast in SOP resonances [25]. The central resonance in I components Figs. 6 (a,c) shows a spectrally broadened transmission peak produced by the transverse field B_y due to coupling between the neighboring Zeeman sublevels. The mismatch in peak heights of the broadened central resonance between the experiment [Fig. 6(a)] and the theory [Fig. 6(c)] is likely caused due to a small magnetic field inhomogeneity present in our experiment. Corresponding dispersive resonances (Q components) are shown in Figs. 6 (b,d).

C. Synchronous CPT spectra in the modulation frequency domain

Next, we show the spectral response of synchronous CPT produced by scanning the modulation frequency Ω_m, and keeping the longitudinal magnetic field B_z fixed. Magnetic resonances generated in this mode, can be utilized in measuring unknown magnetic fields. In Fig. 7, we show the effect of difference detuning

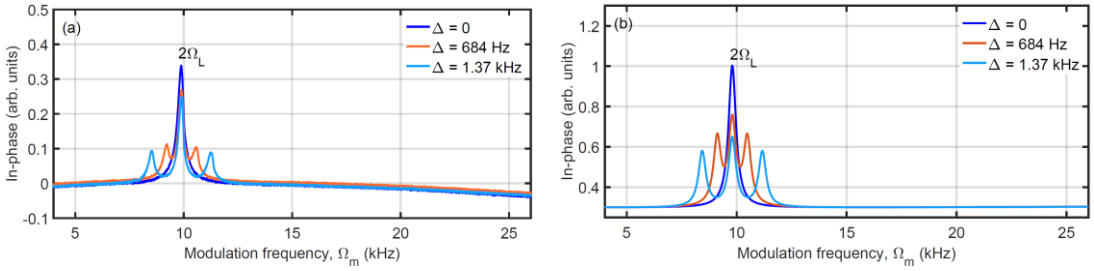

Fig. 7. (a) Experimentally acquired in-phase component of the magnetic resonance signal, obtained by using a constant magnetic field $B_z = 7$ mG and scanning the laser modulation frequency Ω_m. (b) Corresponding theoretical results. A modulated bichromatic laser beam with linear polarization and in resonance with $|F' = 1\rangle$ excited state is used.

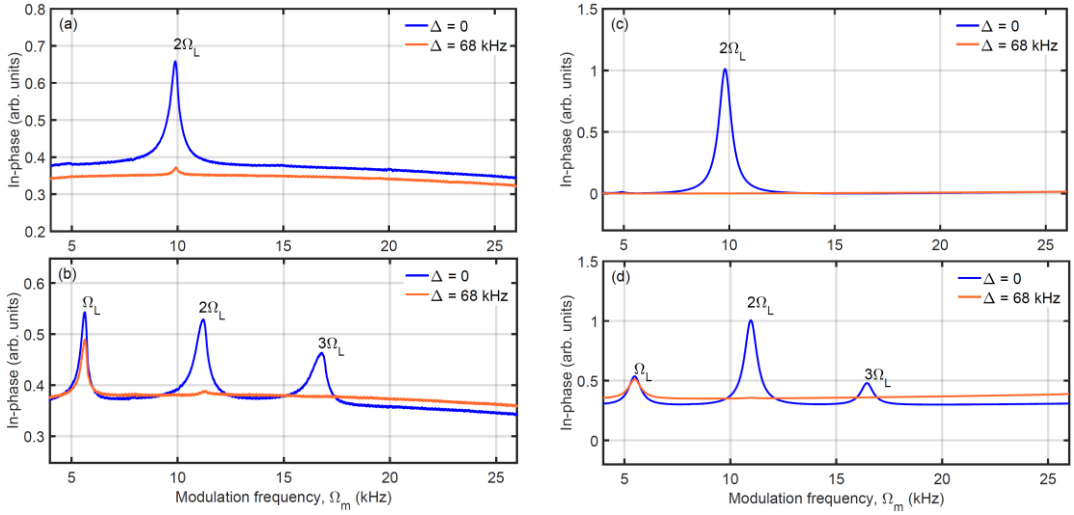

Fig. 8 (a,b) Experimentally acquired in-phase components of magnetic resonance signals for constant magnetic fields (a) $B_z = 7$ mG and (b) $B_x = 2.54$ mG, $B_y = 2.44$ mG and $B_z = 7$ mG. (c,d) Corresponding theoretical results. A modulated bichromatic laser beam with σ^+ polarization and in resonance with the $|F' = 2\rangle$ excited state is used in this case.

Δ on the spectral response of synchronous CPT. A modulated bichromatic linearly polarized laser beam in resonance with $|F' = 1\rangle$ excited state is used. For $\Delta = 0$ case, a strong resonance signal is produced at $\Omega_m = 2\,\Omega_L$ for a longitudinal applied field $B_z = 7$ mG ($\Omega_L \simeq 4.9$ kHz). When a small Δ (i.e. $|\Delta| < \Omega_m$) is introduced between laser frequencies ω_1 and ω_2, two new satellite resonances are formed around the $\Omega_m = 2\Omega_L$ resonance [Figs. 7 (a,b)]. These side-resonances satisfy new two-photon resonance conditions at $\Omega_m = 2\Omega_L \pm \Delta$. Additionally, a SOP resonance at $\Omega_m = 2\,\Omega_L$ is also formed which is confirmed by our theoretical results shown in Fig. 7(b). The amplitude of $2\Omega_L$ SOP resonance is reduced by introducing a Δ larger than the linewidth of $2\Omega_L$ resonance ($\simeq 300$ Hz). For comparison, Fig. 8 shows the magnetic resonance obtained for longitudinal field $B_z = 7$ mG, produced by using a modulated σ^+ polarized laser beam in resonance with $|F' = 2\rangle$ excited state. A strong resonance at $\Omega_m = 2\,\Omega_L$ is produced due to optical pumping by σ^+ polarization. Unlike in the previous case of Fig. 7, we introduce a large Δ [$= 68$ kHz] greater than the $|\Omega_m|$ scan range, in this case. As a result, the satellite two-photon resonances satisfying conditions $\Omega_m = 2\Omega_L \pm \Delta$ are no longer observed. A SOP resonance at $\Omega_m = 2\,\Omega_L$ is also not produced in this case [Figs. 8(a,c)], due to the presence of longitudinal field B_z and excitation using σ^+ polarization. This is consistent with our previous results in Fig. 4. However, due to an imperfection in σ^+ polarization, a weak SOP resonance at $\Omega_m = 2\,\Omega_L$ is observed in our experiment [Fig. 8(a)]. This again illustrates the advantage of synchronous CPT over the SOP technique, for eliminating the dead-zone problem with respect to the longitudinal field B_z [15]. Further, Figs. 8(b,d) show spectral responses produced by synchronous CPT for a general case when a magnetic field is applied in an arbitrary direction [i.e. $B_x = 2.54$ mG, $B_y = 2.44$ mG and $B_z = 7$ mG, and $\Omega_L (= \gamma B) \simeq 5.5$ KHz]. In this case, all three resonance signals at $\Omega_m = \Omega_L, 2\,\Omega_L$ and $3\,\Omega_L$ are produced in the in-phase (I) component. The resonant value of Ω_m for any one of these resonances can be utilized to determine the field strength B. This does not require a calibration of ν_{hfs}. Light shift in synchronous CPT can be much reduced compared to SOP, as well [27]. Intensity ratio between the CPT light fields (i.e. EOM sidebands) can be optimized to reduce the light shift in case of synchronous CPT. This can give an advantage of higher accuracy in the magnetic field measurement. Magnetic field inhomogeneity in our experiment causes progressive broadening of linewidths from Ω_L to $3\,\Omega_L$ resonances. We believe that this is responsible for producing larger peak amplitudes in Ω_L and $3\,\Omega_L$ resonances compared to the theoretically calculated peak amplitudes in Fig. 8(d). In the case of SOP (i.e. $\Delta = 68$ kHz), only one SOP resonance at $\Omega_m = \Omega_L$ is produced. This result also illustrates another advantage of synchronous CPT in producing multiple resonance signals irrespective of the choice of light polarization and the direction of the magnetic field. It is possible to utilize this aspect of synchronous CPT for determining the direction of the magnetic field. For example, variations in relative peak amplitudes between these resonances can be calibrated in terms of light ellipticity and polarization angles. Such calibrations can then be used in determining the magnetic field orientation with respect to the plane of light polarization [14,28]. We plan to study this aspect of synchronous CPT in future for vector field measurement. Additionally, the effect of varying the duty cycle of modulation can also be explored for use in magnetic field measurements.

V. CONCLUSIONS

We investigated the spectral response of synchronous CPT for magnetometry applications by using a bichromatic modulated laser beam excitation in a pure isotope ^{87}Rb vapor. Our study shows that synchronous CPT can provide several advantages in magnetometry without adding any significant complexity to the experimental setup. We systematically examined the spectral differences between synchronous CPT and SOP produced in ^{87}Rb D_1 line using resonant excitation of $|F' = 2\rangle$ excited state with circularly polarized light, and $|F' = 1\rangle$ excited state with linearly polarized light. All of our experimental results are validated using a theoretical model based on the atomic density-matrix equations. We found that synchronous CPT produces a resonant response irrespective of the choice of light polarization and orientation of the magnetic field. This is important in eliminating the dead-zone problem commonly encountered in SOP-based magnetometry. We also showed that for an arbitrarily oriented magnetic field,

multiple resonances are produced in ^{87}Rb D_1 line by the synchronous CPT scheme. This can also be utilized in determining the direction of magnetic field vector in vector magnetometry applications.

ACKNOWLEDGEMENTS

This work is supported by funding received from NASA EPSCoR (80NSSC17M0026), DoD (W911NF1910406) and DoD (W911NF2020276).

[1] F. Renzoni, W. Maichen, L. Windholz, and E. Arimondo, Phys. Rev. A **55**, 3710 (1997).
[2] G. Alzetta, S. Gozzini, A. Lucchesini, S. Cartaleva, T. Karaulanov, C. Marinelli, and L. Moi, Phys. Rev. A **69**, 063815 (2004).
[3] E. Breschi and A. Weis, Phys. Rev. A **86**, 1 (2012).
[4] D. Budker, W. Gawlik, D. F. Kimball, S. M. Rochester, V. V. Yashchuk, and A. Weis, Rev. Mod. Phys. **74**, 1153 (2002).
[5] T. H. Sander, J. Preusser, R. Mhaskar, J. Kitching, L. Trahms, and S. Knappe, Opt. Express **64**, 1759 (2001).
[6] V. Shah and R. T. Wakai, Phys. Med. Biol. 58, 8153 (2013).
[7] W. E. Bell and A. L. Bloom, Phys. Rev. Lett. **6**, 280 (1961).
[8] A. Corney, and G. W. Series, Proc. Phys. Soc. London **83**, 207 (1964).
[9] A. L. Bloom, Appl. Opt.**1**, 61 (1962).
[10] D. Budker, D.F. Kimball, V. V. Yashchuk, and M. Zolotorev, Phys. Rev. A **65**, 055403 (2002)
[11] V. Acosta, M. P. Ledbetter, S. M. Rochester, D. Budker, D. F. Jackson Kimball, D. C. Hovde, W. Gawlik, S. Pustelny, J. Zachorowski, and V. V. Yashchuk, Phys. Rev. A **73**, 053404 (2006).
[12] V. G. Lucivero , P. Anielski , W. Gawlik, and M. W. Mitchell, Rev. Sci. Instrum. **85**, 113108 (2014).
[13] V. V. Yashchuk, D. Budker, W. Gawlik, D. F. Kimball, Y. P. Malakyan, and S. M. Rochester, Phys. Rev. Lett. **90**, 2530011 (2003).
[14] R. S. Grewal, G. Pati, R. Tripathi, Phys. Rev. A 102, 033102 (2020).
[15] Z. D. Grujić and A. Weis, Phys. Rev. A **88**, 1 (2013).
[16] E. Breschi, Z. D. Grujic, P. Knowles, and A. Weis, Appl. Phys. Lett. **104**, 1–5 (2014)
[17] S. A. Zibrov, I. Novikova, D. F. Phillips, R. L. Walsworth, A. S. Zibrov, V. L. Velichansky, A. V. Taichenachev, and V. I. Yudin, Phys. Rev. A - At. Mol. Opt. Phys. **81**, 1–7 (2010).
[18] Z. Warren, M.S. Shahriar, R. Tripathi, and G.S. Pati, Metrologia **54**, 418 (2017).
[19] P. D. D. Schwindt, S. Knappe, V. Shah, L. Hollberg, J. Kitching, L.A. Liew, and J. Moreland, Appl. Phys. Lett. **85**, 6409 (2004).
[20] R. Tripathi, and G.S. Pati, IEEE Photonics J. **11**, 1 (2019).
[21] R. S. Grewal, M. Pulido, G. Pati, R. Tripathi, Appl. Phys. Lett. **117**, 214002 (2020).
[22] M. S. Shahriar, Y. Wang, S. Krishnamurthy, Y. Tu, G. S. Pati, and S. Tseng, J. Mod. Opt. **61**, 351–367 (2014).
[23] S. M. Rochester, see http://rochesterscientific.com for 'Atomic Density Matrix Package'.
[24] L. Margalit, M. Rosenbluh, and A. D. Wilson-Gordon, Phys. Rev. A **88**, 023827 (2013).
[25] Z. Y. Jiang, X. C. Liu, P. W. Lin, J. F. Qu, and H. P. Liu, Opt. Lett. **45**, 105 (2020).
[26] A. Ben-Kish and M. V. Romalis, Phys. Rev. Lett. **105**, 3 (2010).
[27] G. S. Pati, Z. Warren, N. Yu, and M. S. Shahriar, J. Opt. Soc. Am. B **32**, 388 (2015).
[28] K. Cox, V. I. Yudin, A. V. Taichenachev, I. Novikova, and E. E. Mikhailov, Phys. Rev. A 83, 015801 (2011).